PAPER

N-doped monolayer graphene catalyst on silicon photocathode for hydrogen production†

Uk Sim,‡[a] Tae-Youl Yang,‡[a] Joonhee Moon,‡[b] Junghyun An,[a] Jinyeon Hwang,[a] Jung-Hye Seo,[c] Jouhahn Lee,[c] Kye Yeop Kim,[a] Joohee Lee,[a] Seungwu Han,[a] Byung Hee Hong*[b] and Ki Tae Nam*[a]

Carbon-based catalysts have been attracting attention in renewable energy technologies due to the low cost and high stability, but their insufficient activity is still a challenging issue. Here, we suggest that monolayer graphene can be used as a catalyst for solar-driven hydrogen evolution reaction on Si-photocathodes, and its catalytic activity is boosted by plasma treatment in N_2-ambient. The plasma treatment induces abundant defects and the incorporation of nitrogen atoms in the graphene structure, which can act as catalytic sites on graphene. The monolayer graphene containing nitrogen impurities exhibits a remarkable increase in the exchange current density and leads to a significant anodic shift of the onset of photocurrent from the Si-photocathode. Additionally, monolayer graphene shows the passivation effect that suppresses the surface oxidation of Si, thus enabling the operation of the Si-photocathode in neutral water. This study shows that graphene itself can be applied to a photoelectrochemical system as a catalyst with high activity and chemical stability.

Broader context

Hydrogen production from solar energy is an important energy and environmental issue. Silicon, one of the most abundant elements, has been widely studied as a cathode for photoelectrochemical hydrogen production. However, the catalyst is necessary to improve conversion efficiency by reducing high overpotential for hydrogen evolution from water. Carbon-based catalysts are attractive candidates due to their low cost and high stability. In this work, our study shows that N-doped monolayer graphene acts as a catalyst for hydrogen production and is better than other carbon catalysts in aspects of overpotential, current density and long-term stability. This approach shows the importance of controlling defects and dopants in graphene to improve catalytic activity. Moreover, these findings can be applied to the use of graphene catalysts for other electrochemical reactions in various energy conversion systems.

Introduction

The discovery of efficient catalysts represents one of the most important and challenging issues for the implementation of photoelectrochemical hydrogen production.[1] A critical requirement for outstanding catalysts in a photoelectrochemical cell (PEC) is not only the ability to boost the kinetics of a chemical reaction but also durability against electrochemical and photoinduced degradation.[2] Generally, precious metals, such as platinum, exhibit superior performance in these requirements; however, the unavoidable weaknesses of precious metals are the economic aspects because of the high-price.[1] Therefore, there

has been an intense search for efficient, durable, and inexpensive alternative catalysts.[2,3] Here, we demonstrate that monolayer graphene can catalyze the hydrogen evolution reaction (HER); thus, monolayer graphene can enhance the performance of silicon (Si) photocathodes through a significant decrease in the overpotential. The catalytic activity can be improved in N-doped and defect-abundant graphene that was prepared by treatment with N_2 plasma. Furthermore, surface passivation with a transparent monolayer graphene catalyst allows the Si photocathode to work efficiently and stably in neutral water by suppressing oxidation.

A PEC is the most promising system to sustainably produce hydrogen fuel; a PEC requires semiconductor photoelectrodes that generate electron–hole pairs with absorbed photons and stimulate charge transfer to a semiconductor–aqueous interface.[1] To improve the kinetics of charge transfer, heterogeneous catalysts are added to the surface of a semiconductor.[4] Many attempts to develop highly efficient catalysts have had limited success; the development of an earth-abundant catalyst that operates at pH 7 with a low overpotential is still a challenge.[2,5] In PEC, negative effects from catalysts should be considered: (1)

[a]Department of Materials Science & Engineering, Seoul National University, 1 Gwanak-ro, Gwanak-gu, Seoul, 151-744, Korea. E-mail: nkitae@snu.ac.kr; Fax: +82-2-887-6388; Tel: +82-2-880-8305

[b]Department of Chemistry, Seoul National University, 1 Gwanak-ro, Gwanak-gu, Seoul, 151-744, Korea. E-mail: byunghee@snu.ac.kr; Tel: +82-2-880-6559

[c]Korea Basic Science Institute, Daejeon, 305-806, Korea

† Electronic supplementary information (ESI) available: Additional information, figures, and table. See DOI: 10.1039/c3ee42106f

‡ These authors contributed equally to this work.

reflection by the overlaid catalyst, (2) an unfavorable band structure such as a Schottky barrier (3) photocorrosion, and (4) recombination sites at the interface.[6,7] Therefore, to design catalysts for photoelectrochemical water splitting, the optical properties, stability and interfacial issues must be comprehensively considered.

The design of carbon-based catalysts represents an important research direction in the search for non-precious, environmentally benign, and corrosion resistant catalysts. Especially, graphene possesses excellent transmittancy and superior intrinsic carrier mobility;[8] thus there have been several attempts to use graphene as a catalyst. It has been reported that reduced graphene oxide (rGO) containing catalytic active materials exhibited improved activity in HERs, oxygen evolution reactions (OERs), and oxygen reduction reactions (ORRs).[9–11] However, in most cases, the role of carbon materials is limited to an electrical conducting substrate or a support that enhances the performance of other decorated active catalysts. In this study, we investigated new possibilities for monolayer graphene as an electrocatalyst for efficient HER and found that nitrogen doping and defects achieved through treatment with N_2 plasma improved the catalytic activity. To the best of our knowledge, there is no prior report on the application of monolayer graphene to hydrogen production.

As a proof of concept, the Si photocathode was employed to investigate the catalytic activity of graphene and the effect of nitrogen doping in photoelectrochemical HER. Si is the most promising photocathode material due to the small band gap of 1.12 eV and precise controllability;[12] however, it cannot be durably operated in aqueous electrolytes because of surface oxidation.[13] Therefore, passivation of Si surface is essential for the durable operation of the Si photocathode in neutral water.[13] Monolayer graphene on Si acts as a passivation layer against surface oxidation without attenuating the photon incidence.

Results and discussion

Monolayer graphene (Gr) was grown on Cu foil through chemical vapor deposition (CVD) and was transferred to a p-type Si wafer. To evaluate the photocathodic behavior of Gr loaded on a Si (Gr–Si) electrode, a current density measurement was performed as the potential was swept from 0.4 V to −1.0 V vs. Reversible Hydrogen Electrode (RHE) in a three electrode cell. A light source of a 300 W Xe lamp illuminated the Si photoelectrode with a light intensity of 100 mW cm^{-2} with an Air Mass 1.5 Global condition filter in an aqueous 1 M perchloric acid solution (pH 0).

In measurements of the photoelectrochemical performance, Gr exhibits catalytic activity for HER. As shown in Fig. 1a, the current density of the bare Si increases gradually from −0.2 V vs. RHE and is saturated at approximately −32 mA cm^{-2} below −1.0 V vs. RHE, as a potential is negatively applied. Interestingly, in the measurement of Gr–Si, the overall current density–potential (J–E) curve is shifted by approximately 0.2 V toward the positive potential. The onset potential is defined as the potential at the photocurrent density of −1 mA cm^{-2}. The onset potential of Gr–Si is 0.01 V vs. RHE, and this potential is a
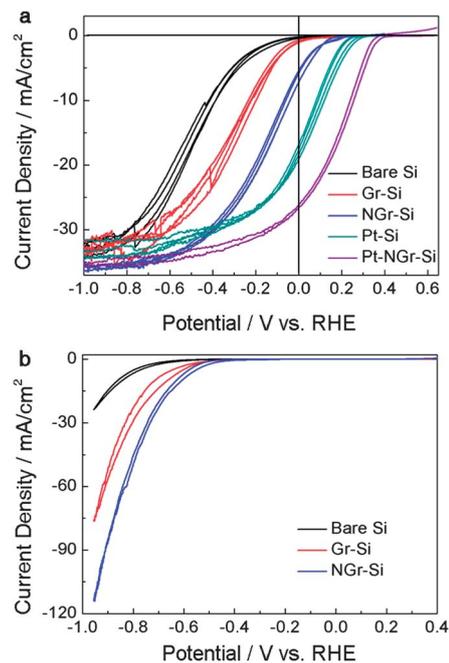
Fig. 1 Cyclic Voltammetry (CV) of graphene (Gr), N_2-plasma-treated Gr (NGr), Pt, and Pt with NGr on a Si electrode. (a) Photocurrent density–potential (J–E) curves for the lightly boron doped p-Si electrode deposited with Gr and NGr. The plasma treatment on Gr was introduced with high purity N_2 gas for a duration of 14 s, which is called NGr–Si. In the case of Pt–Si and Pt–NGr–Si electrodes, Pt nanoparticles were deposited on bare Si and NGr–Si by the electroless deposition method, respectively. (b) Polarization curves of Gr and NGr on heavily arsenic doped n$^+$ type Si electrodes under dark conditions. Each CV process was performed at a scan rate of 0.05 V s^{-1}.

positive shift by 0.18 V compared to that of bare Si (−0.17 V vs. RHE). Fig. 1b also shows dark current densities of heavily arsenic doped n$^+$ type Si electrodes. In dark conditions, the positive shift in 0.14 V of the onset potential (−0.49 V vs. RHE for Gr–Si) also shows higher activity for HER compared to that of the bare Si (−0.63 V vs. RHE). This result indicates that monolayer Gr acts as an effective catalyst for HER on the Si photocathode.

To investigate the electrocatalytic activity of Gr, we performed cyclic voltammetry (CV) without illumination with a rotating disk electrode (RDE). To fabricate the working electrode, Gr was transferred to a glassy carbon (GC) tip that is inert in aqueous solution. As shown in Fig. 2a, in J–E curves of the RDE measurements, the current density from the electrolysis of water exponentially increases after the onset as the potential is swept from 0 V to −0.5 V. To compare the onset potential for the HER in the RDE system, the potential to attain −5 mA cm^{-2} of HER current density was measured for bare GC and for Gr–GC. The potential to attain −5 mA cm^{-2} of HER current density is −0.33 V for the bare GC. Similar to the behavior of the photocurrent response for the Gr–Si electrode, a positive shift in the overall J–E curve is also observed for Gr–GC. The potential for Gr–GC at −5 mA cm^{-2} is −0.28 V vs. RHE; this potential is shifted positive by 50 mV compared to that for the bare GC. This result means that the Gr monolayer has electrocatalytic activity for HER regardless of substrate materials.
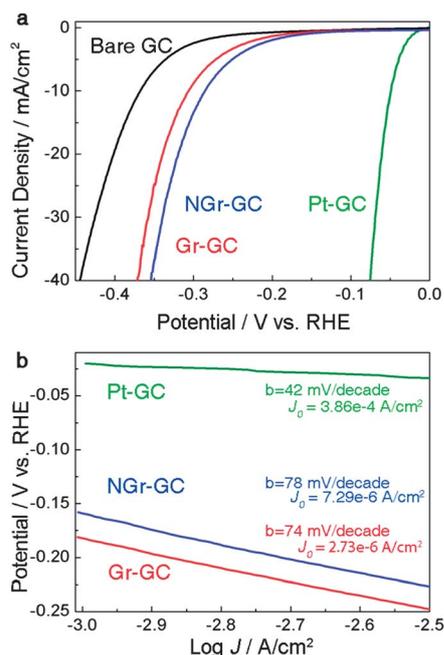
Fig. 2 Electrochemical activity of Gr on a Glassy Carbon (GC) electrode. (a) CV curve of GC, Gr on GC, NGr on GC, and Pt on GC from a rotating disk electrode system. CV data were corrected by iR compensation. (b) Tafel plots were derived from (a) CV data. The 'b' (mV per decade) and J_0 (A cm^{-2}) in the inset indicate a Tafel slope and an exchange current density, respectively.

To quantitatively gain more insight into the catalytic activity of Gr, the J–E curves in Fig. 2a is converted into a plot of the potential as a function of the logarithm of J; this plot is called a Tafel plot. The measured potentials are corrected for the ohmic potential drop (iR) losses that originated from the resistance of the interface between the substrate and the electrolyte. Analyzing the impedance spectroscopy reveals that the resistances of the bare GC and Gr–GC are 7.1 and 7.2 ohm, respectively (Fig. S2†). The Tafel plot provides two parameters to estimate the electrocatalytic activity: the Tafel slope and the exchange current density. The Tafel slope is defined to be a measure of the potential increase required to increase the resulting current by 1 order of magnitude.[14] The bare GC shows a Tafel slope of 85 mV per decade, and Gr–GC exhibited a 9 mV per decade lower Tafel slope (74 mV per decade) than that of bare GC. For the comparison with the well-known catalyst, Pt particles were deposited on GC and the electro-catalytic activity was analysed. The applied potential to obtain -5 mA cm^{-2} is -0.04 V vs. RHE, which is shifted positively by 0.24 V compared to that of Gr–GC. The Tafel slope of Pt–GC is 42 mV per decade, which is 32 mV per decade lower than that of Gr–GC. In the case of the 2D MoS$_2$ catalyst, the potential to attain -5 mA cm^{-2} is -0.19 V vs. RHE and the Tafel slope was 60 mV per decade when deposited as a mixture with Nafion on GC.[15]

The Tafel slope is an inherent property of the catalyst that is determined by the rate-limiting step for HER. Mechanistically, for the HER in acidic solution, the following possible reaction steps have been suggested:[16]

$$H_3O^+ + e^- \rightarrow H_{ads} + H_2O \quad (1)$$

$$H_{ads} + H_3O^+ + e^- \rightarrow H_2 + H_2O \quad (2)$$

$$H_{ads} + H_{ads} \rightarrow H_2 \quad (3)$$
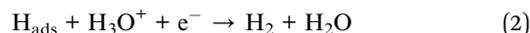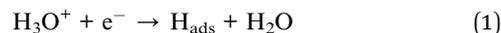
where H_{ads} is the adsorbed hydrogen. (1) is a discharge step (the Volmer reaction), (2) is a desorption step (the Heyrovsky reaction), and (3) is a recombination step (the Tafel reaction). The value of the Tafel slope also relates to the adsorbed hydrogen coverage (θ_H) on the surface of the electrode. If the recombination of adsorbed hydrogen (the Tafel reaction) is the rate-determining step for the HER and if the coverage is very high ($\theta_H \approx 1$), the measured Tafel slope is 30 mV per decade. However, if the electrochemical desorption step (the Heyrovsky reaction) is the rate-determining step, a Tafel slope of 40–118 mV per decade is measured and is dependent on the value of θ_H ($0 \sim 1$).[17] The observed Tafel slope of $\sim$80 mV per decade in the current work indicates that the kinetics of the HER on bare GC and Gr–GC electrodes is determined by the Heyrovsky reaction because θ_H has an intermediate value.

The exchange current density (J_0) is defined to be the current density at zero overpotential. The catalytic effect originates from improving the rate of charge transfer at the interface between the electrode and the electrolyte or from lowering the activation energy barrier for a chemical reaction; these catalytic effects are represented by J_0. The higher J_0 indicates that electron transfer or the adsorption/desorption of protons at the electrode/electrolyte can occur more easily with a lower kinetic barrier. From the Tafel plot, J_0 can be obtained by extrapolating the plot in Fig. 2b and extracting the current density at 0 V vs. RHE. The Gr–GC electrode shows an enhanced J_0 of 2.73×10^{-6} A cm^{-2}, which is higher than the J_0 of bare GC (1.63×10^{-6} A cm^{-2}) (Fig. S3†). The J_0 of the monolayer Gr is also compared with that of the nanoparticulate MoS$_2$. The accurate J_0 can be calculated by considering the number of active sites. For example, the J_0 of MoS$_2$ for HERs is experimentally measured to be 1.3×10^{-7} to 3.1×10^{-7} A cm$_{geometric}^{-2}$.[18] Active sites of MoS$_2$ nanoparticles for HER are known to be edge sites of MoS$_2$ nanoparticles.[16,18] For the direct site-to-site comparison between MoS$_2$ nanoparticle and Pt catalyst, T. Jaramillo et al. have measured an exchange current per site of MoS$_2$ combined with STM analysis.[18] The exchange current per site is then multiplied by the site density of Pt for a fair comparison to the transition metal catalyst, resulting in the exchange current density of 7.9×10^{-6} A cm^{-2}. This value is still similar to the exchange current density of Gr (2.7×10^{-6} A cm^{-2}). We are currently investigating to identify and quantify the active sites of the single monolayer Gr. From the Tafel analysis, Gr has the catalytic activity for the HER compared to that of the nanoparticulate MoS$_2$.

The catalytic activity of Gr can be further enhanced by generating more active sites. We expected that treatment with N$_2$ plasma would induce nitrogen doping and abundant defects in the graphitic carbon structure and that these doping and defect sites could be catalytic sites for the HER. In a previous study, Dai's group showed that introducing nitrogen dopants and defect sites in a CNT–Gr composite facilitated an improvement in

3660 | Energy Environ. Sci., 2013, **6**, 3658–3664

This journal is © The Royal Society of Chemistry 2013

electrocatalytic activity for ORR.[19] The surface of the as-grown Gr on Cu foil was modified with N_2 plasma in a reactive ion etcher (RIE), and the catalytic activities of the N_2-plasma-treated Gr (NGr) were measured for various durations of the plasma treatment.

The N_2-plasma treatment improved the catalytic activity of Gr. We optimized the duration of the plasma treatment, and obtained the best-performing Gr at the duration of 14 s (Fig. 1a and S4†). As shown in Fig. 1a, an additional positive shift of the onset potential is observed for NGr under illumination. The onset potential for NGr–Si is 0.12 V *vs.* RHE, and this onset potential is enhanced by more than 0.11 V compared to that for Gr–Si. In comparison to bare Si with the onset of −0.17 V *vs.* RHE, the onset potential is shifted positively by 0.29 V. The more significant enhancement by Gr and NGr is detected at a current density of −10 mA cm^{-2}. To obtain −10 mA cm^{-2} of photocurrent, potentials of −0.42 V, −0.21 V, and −0.04 V *vs.* RHE are needed for bare Si, Gr–Si, and NGr–Si, respectively. The potential for −10 mA cm^{-2} is shifted to the anodic direction by 0.38 V for NGr–Si compared with bare Si. The cathodic current from NGr–Si rises rapidly at potentials more negative than the onset potential and at current densities less than −5 mA cm^{-2}. In dark conditions, NGr–Si also shows the positive shift in 50 mV (−0.44 V *vs.* RHE) compared to the Gr–Si (Fig. 1b), which results in the photovoltage of 0.56 V by depositing NGr on bare Si (Table S1†). For comparing the catalytic activity of NGr with that of the best catalyst, the CV of Si with electroless-deposited Pt (Pt–Si) is also measured (Fig. 1a). The onset of Pt–Si is 0.24 V *vs.* RHE, and the potential to obtain −10 mA cm^{-2} is 0.11 V *vs.* RHE, which is the

positive shift in 0.12 V *vs.* RHE compared to that of the NGr–Si electrode. NGr–Si is also compared to the Si electrode decorated with an earth abundant catalyst, Ni.[20] The Ni–Si electrode shows a solar-to-hydrogen (STH) conversion efficiency of 0.4% with the onset potential of 0.34 V *vs.* RHE and *J* at 0 V *vs.* RHE of 10 mA cm^{-2}. NGr–Si shows the onset potential (0.12 V *vs.* RHE) and *J* at 0 V *vs.* RHE (−5.5 mA cm^{-2}). Consequently, the STH conversion efficiency (+0.16%) is achieved by using the NGr catalyst (Table S1†). NGr–Si is also compared with the Si electrode with MoS_2 catalyst. The photocurrent density at 0 V *vs.* RHE of NGr on the Si electrode is much higher (−5.5 mA cm^{-2}) than the reported value of MoS_2 (approximately −0.5 mA cm^{-2}).[21]

An additional positive shift in the onset potential by NGr is also observed in the RDE measurements. The potential to attain a current density of −5 mA cm^{-2} is −0.26 V *vs.* RHE; this value is 70 mV larger than that of the bare GC (−0.33 V *vs.* RHE) and is 20 mV larger than that of the Gr–GC (−0.28 V *vs.* RHE). The improvement in the catalytic activity with NGr is also confirmed by the comparison of J_0 in the Tafel plot (Fig. 2b). The J_0 of NGr–GC is 7.29×10^{-6} A cm^{-2}, which is approximately 2.8 times higher than that of Gr–GC. This is a comparable value with that of the nanoparticulate MoS_2 (7.9×10^{-6} A cm^{-2}).[18]

In Fig. 3, we describe the changes in chemical states of Gr after N_2 plasma treatments for various durations. AFM images of the surface of NGr with N_2 treatment for 14 s show that plenty of defects and edges were generated in the Gr, while that of monolayer Gr was smooth (Fig. S5†). In the Raman spectra (Fig. 3a), the generation of defects and edges by the N_2
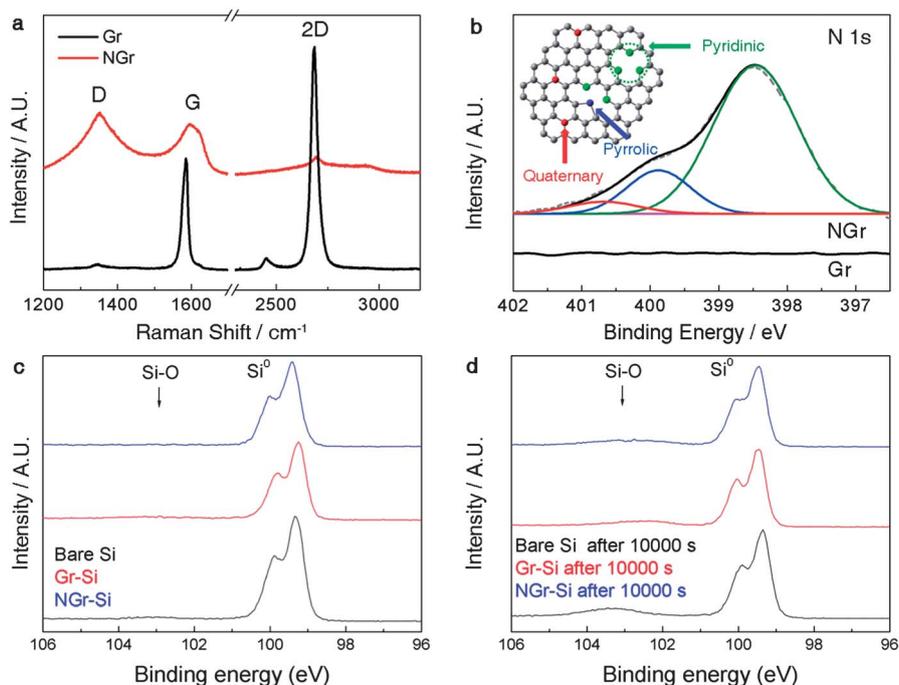
Fig. 3 (a) Raman spectra and (b) high resolution XPS spectra of N 1s peak of Gr and NGr. The N 1s peak is separated into pyridinic N (398.5 eV), pyrrolic N (399.9 eV), and quaternary N (401 eV), which are labeled by green, blue, and red lines. An inset image in (b) represents the schematic of NGr. The gray, green, blue, and red spheres indicate the carbon, pyridinic nitrogen, pyrrolic nitrogen, and quaternary nitrogen atoms, respectively. (c and d) High resolution XPS spectra of the Si 2p region of bare Si (black line), Gr–Si (red line), and NGr–Si (blue line) electrodes. XPS spectra of each sample (c) before the chronoamperometry test and (d) after the chronoamperometry test at 0 V *vs.* RHE for 10 000 s. Narrow-scan data of the Si 2p region were collected using a pass energy of 40 eV and 0.05 eV per step.

This journal is © The Royal Society of Chemistry 2013

Energy Environ. Sci., 2013, **6**, 3658–3664 | **3661**

treatment is also identified. In the Raman spectra of pristine Gr, the D peak is due to the breathing modes of six-atom rings, which comes from transverse optical phonons around the K or K' point in the first Brillouin zone. It involves an intervalley double resonance process. The absence of a significant D peak is the evidence of the good crystallization of the single Gr layer. In monolayer graphene with good crystallinity, the D peak is negligibly weak in pristine Gr, but the D peak is still as high as approximately 2% of the G peak, which can be good active sites for hydrogen production. However, after the plasma treatment, the intensity of the D peak significantly increases and the D′ peak at ~1620 cm^{-1} is activated by the intravalley double resonance process, i.e., connecting two points that belong to the same cone around K or K'. Moreover, the D + G combination mode at ~2950 cm^{-1} requires defects for its activation.[22] Thus, these changes in the Raman spectra indicate the formation of abundant edges and defective sites in NGr.

Additionally, the spectral features of monolayered Gr are observed in the Raman spectra. Before the plasma treatment, the G to 2D intensity ratio of ~0.5 and a symmetric 2D band are found at ~1580 cm^{-1} and ~2670 cm^{-1}.[23] These features are caused by the G band from the in-plane vibrational mode and the 2D band from double resonance scattering, respectively.[24,25] Thus, they can be observed when Gr is successfully formed in a single-layer.

The plasma treatment induces not only the formation of many defect sites but also nitrogen doping in Gr. The chemical states of the nitrogen dopant were identified from the high resolution N 1s spectra from X-ray photoelectron spectroscopy (XPS, Fig. 3b and S6†). No obvious distinct nitrogen peak is observed for Gr, whereas nitrogen peaks for NGr are observed at pyridinic (398.5 eV), pyrrolic (399.9 eV), and a small number of quaternary nitrogen (401 eV) sites with a concentration of ~2.2 at%. The inset in Fig. 3b shows a schematic diagram of the bonding configurations for nitrogen in NGr.

The passivation effect of Gr was also investigated. CV of Si photocathodes was measured during 300 cycles with a scan rate of 0.05 V s^{-1} (Total operation time of each electrodes is approximately 20 000 s) in pH 0 and pH 6.8. As shown in Fig. 4a and b, CV curves of all electrodes shift negatively vs. RHE as the CV cycle increases, but bare Si shows the largest negative shift

even in much lower cycles. As a key parameter determining the passivation performance of Gr and NGr against the surface oxidation of Si, the changes in onset potentials were measured (Fig. S7†). At pH 0, the Gr–Si and NGr–Si electrodes shows only shifts in the onset potential of 0.1 V and 0.035 V, respectively, while the onset potential of the bare Si electrode shifts negatively by 0.38 V within 100 cycles (Fig. S7†). At pH 6.8, both the Gr–Si and NGr–Si electrodes show the negative shift of less than 0.24 V in the onset potential, whereas the onset potential of the bare Si sharply decreases and is saturated at a value of approximately −1.1 V vs. RHE within only 30 cycles.

A chronoamperometry test of the bare Si, Gr–Si, and NGr–Si was also performed at 0 V vs. RHE (Fig. S8†) and the current densities normalized by their initial values are displayed as a function of time in Fig. 4c. Gr–Si and NGr–Si also show the suppressed degradation of the performance in the photocurrent density compared to that of the bare Si at both pH 0 and pH 6.8 conditions. The performance of the bare Si completely fails only after 1000 s (Fig. 4c and S8†) at pH 6.8. The NGr–Si electrode maintains more than 30% of the normalized current and −4.8 mA cm^{-2} (pH 0) even at 10 000 s. Thus, from the change of the onset potential and current density at 0 V vs. RHE, it is known that Gr and NGr suppress the degradation of the photoelectrochemical performance by the oxidation of the Si surface.

To confirm the passivation effect of Gr and NGr on the Si surface, the surface state of Si was investigated before and after the chronoamperometry test at 0 V vs. RHE for 10 000 s (Fig. 3c and d). XPS spectra of bare Si, Gr–Si, and NGr–Si were obtained in the Si 2p$_{3/2}$ region. The Si peak can be assigned at 99.3 eV, and the SiO$_2$ peak can be assigned at 103.3 eV.[26] From XPS spectra of bare Si, the peak of Si–O increases after the chronoamperometry test. In the case of Gr–Si and NGr–Si samples, after the long-term test, there is only a slight increase in the Si–O peak. These results indicate that graphene suppresses the oxidation of the Si surface during photoelectrolysis.

To further enhance the electro-catalytic activity of Gr, Pt nanoparticles were electrodeposited onto the NGr–Si (Pt–NGr–Si). We also expected that the passivation effect of Gr to suppress the Si oxidation during the photoelectrolysis could make the synergistic advantage with other catalysts. As a proof of concept, Pt was chosen to investigate those effects. The
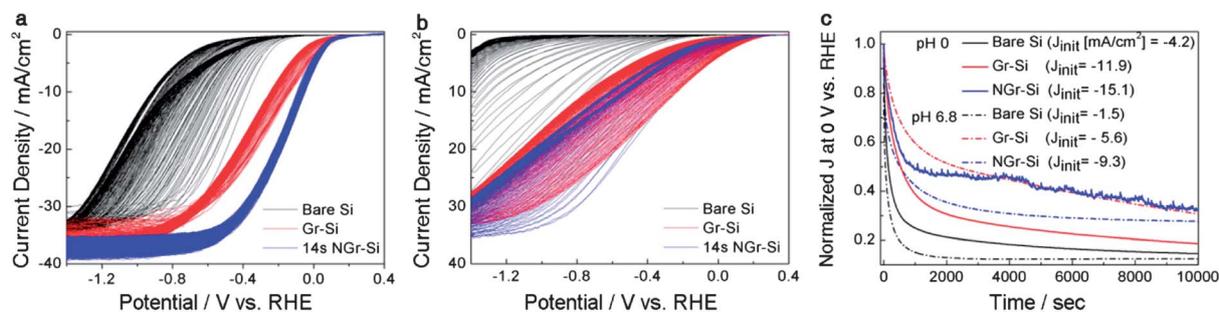
Fig. 4 The stability test of bare Si, Gr–Si, and NGr–Si photocathodes. CV of Si photocathodes during 300 cycles with a scan rate of 0.05 V s^{-1} at (a) pH 0 and (b) pH 6.8. Polarization curves of each photoelectrode shifted negatively vs. RHE as the CV operation increased. (c) Chronoamperometry operation of photocathodes. The change of the photocurrent densities at 0 V vs. RHE normalized by their initial value (J/J_{init}) for each photoelectrode with the increase of time at pH 0 (solid line) and pH 6.8 (dash-dotted line), respectively. J_{init} is the initial current density in the chronoamperometry operation.

3662 | Energy Environ. Sci., 2013, **6**, 3658–3664

This journal is © The Royal Society of Chemistry 2013

catalytic activity of Pt–NGr–Si was significantly enhanced compared to that of NGr–Si as shown in Fig. 1a. From a CV measurement, the onset of Pt–NGr–Si is 0.35 V *vs.* RHE at −1 mA cm^{-2}, and the potential to reach −10 mA cm^{-2} is 0.25 V *vs.* RHE. The STH conversion efficiency is increased to 3.05%. As expected, the long-term stability was also achieved by combining Pt and Gr as demonstrated in Fig. S10 and S11.† The chronoamperometry test showed that Pt–NGr–Si maintained the stable current density of −4.7 mA cm^{-2} and −4.0 mA cm^{-2}, respectively, at pH 3.8 and 6.8 even after 8000 s.

Conclusion

We have presented the N-doped monolayer graphene catalyst that enhanced the PEC performance of a Si-photocathode. The onset potential for photocurrent from the Si was significantly shifted toward the anodic direction without a change in the saturation current density. NGr has excellent catalytic activity for photoelectrochemical HER on the Si photocathode and is the passivation layer that maintains higher onset potential and current density even at neutral pH. Our approach in this study exploits a strategy to develop metal-free carbon-based catalysts with high efficiency and durability for solar-driven hydrogen fuel production.

Experimental

Synthesis of graphene

A monolayer graphene was grown on Cu foil by chemical vapor deposition (CVD) and then transferred to a SiO$_2$ surface. In the first step of graphene synthesis, a copper foil was put into a quartz reactor in the CVD system and then heated to 1000 °C with flowing H$_2$ at 70 mTorr. Additionally, the sample was annealed for 20 min without changing the condition. The gas mixture of H$_2$ and CH$_4$ was flowed with rates of 5 and 50 SCCM for 30 min under 8 Torr. Finally, the sample was rapidly cooled down to room temperature with flowing H$_2$. After growth, in order to remove graphene on one of the sides of Cu foil, graphene on Cu was placed into the plasma chamber (SNTEK). The chamber pressure was pumped down to 50 mTorr, and O$_2$ gas was introduced into the chamber by applying a radio-frequency (13.56 MHz) forward power of 100 W for 10 s. In addition, to make vacancy sites and N-doping graphene on the front side of Cu, low density N$_2$-plasma was produced by applying 10 W power. The N$_2$ flow rate was 20 SCCM and the working pressure of the chamber was 120 mTorr. Under these conditions, the plasma treatments were performed with various exposure times from 0 to 16 s of N$_2$ plasma to test the electrochemical reaction of the graphene surface. Finally, poly(methyl methacrylate) (PMMA) was spin-coated on graphene and then copper foil was removed in 0.1 M ammonium persulfate solution. After washing with deionized water, the graphene was transferred onto the Si substrate and then PMMA was removed in acetone for 30 min.

Preparation of Si photocathode

In order to establish an ohmic contact between copper wire and the unpolished side (back side) of the Si wafer, a gallium–indium eutectic alloy was incorporated followed by the silver paste. The epoxy was used to insulate and protect the back contact of Si except for the intended illumination area (0.25 cm^2) of the Si front side. Gr was transferred to the Si surface from Cu foil. PMMA was spin-coated on Gr and then the copper foil was removed in an ammonium persulfate solution. After washing with deionized water, Gr was transferred onto the Si substrate and then PMMA was removed in acetone for 30 min.

Electrochemical measurements

Electrochemical measurements were performed in a three-electrode cell using an electrochemical analyzer (CHI 600D, CH Instruments, Inc.). Pt foil was used as the counter electrode and Ag/AgCl/3 M NaCl electrode was used as the reference electrode. The reference electrode was carefully calibrated with respect to RHE in an aqueous 1 M perchloric acid solution with high purity H$_2$ saturation at 25 °C (Fig. S1†). The RHE was calibrated to between −0.201 V and −0.203 V *vs.* the Ag/AgCl reference electrode. To evaluate the photoelectrochemical behavior, visible light from a 300 W Xe lamp was illuminated onto the substrate with the light intensity of 100 mW cm^{-2} using an Air Mass 1.5 Global condition glass filter. The RDE system was purchased from EG&G PARC Inc and Glass Carbon tip for RDE measurement (dia. 3 mm) was purchased from BASi. The Pt catalyst mixed with 5 wt% Nafion was synthesized from the literature method.[16] The Pt catalyst ink of 10 uL was loaded on GC and dried at 110 °C. RDE measurement was performed at a rotating speed of 1000 rpm with a scan rate of 5 mV s^{-1}.

Calibration with respect to relative hydrogen electrode

The Ag/AgCl/3 M NaCl electrode (BASi) was used as the reference electrode. Pt foil (2 cm × 2 cm × 0.1 mm, 99.997% purity, Alfa Aesar) was used as the counter electrode. In the case of RDE experiment, Pt wire (0.1 mm diameter, Dr Bob's cell) was used as the counter electrode. It was carefully calibrated with respect to the reversible hydrogen electrode (RHE) in an aqueous 1 M perchloric acid solution (Sigma Aldrich) with high purity H$_2$ saturation at 25 °C. The RHE was calibrated to between −0.201 V and −0.203 V *vs.* the Ag/AgCl reference electrode (Fig. S1†). Since the potential difference between Ag/AgCl and RHE is dependent on electrolyte pH, temperature, and so on, the potential was carefully measured before each set of measurement and the measurement was conducted at least three times for each condition. The potential was controlled using a potentiostat (CHI 600D, CH Instrument) at a scan rate of 5 mV s^{-1}.

Characterization

Raman spectra were obtained with a Renishaw micro-Raman spectroscope with an excitation wavelength of 514.5 nm, an Ar laser. The spot diameter was approximately 2 μm with a 50× objective lens. The oxygen plasma treatment (SNTEK) was carried out with a 100 W radio-frequency (rf) power for 13 s under 140 mTorr and the nitrogen plasma was accelerated with a 10 W rf power for several exposure times (0 to 16 s) under 120 mTorr. XPS spectra were collected by AXIS Ultra DLD (Kratos. Inc) using a monochromatic Al K (1486.6 eV), 150 W

This journal is © The Royal Society of Chemistry 2013

Energy Environ. Sci., 2013, **6**, 3658–3664 | **3663**

source at Korea Basic Science Institute (KBSI). Narrow-scan data were collected using a pass energy of 40 eV and 0.05 eV per step.

Acknowledgements

References

1 A. Heller, E. Aharon-Shalom, W. A. Bonner and B. Miller, *J. Am. Chem. Soc.*, 1982, **104**, 6942–6948.

2 Y. Hou, B. L. Abrams, P. C. K. Vesborg, M. E. Björketun, K. Herbst, L. Bech, A. M. Setti, C. D. Damsgaard, T. Pedersen, O. Hansen, J. Rossmeisl, S. Dahl, J. K. Nørskov and I. Chorkendorff, *Nat. Mater.*, 2011, **10**, 434–438.

3 S. Y. Reece, J. A. Hamel, K. Sung, T. D. Jarvi, A. J. Esswein, J. J. H. Pijpers and D. G. Nocera, *Science*, 2011, **334**, 645–648.

4 A. Kudo and Y. Miseki, *Chem. Soc. Rev.*, 2009, **38**, 253–278.

5 Y. W. Chen, J. D. Prange, S. Dühnen, Y. Park, M. Gunji, C. E. Chidsey and P. C. McIntyre, *Nat. Mater.*, 2011, **10**, 539–544.

6 R. N. Dominey, N. S. Lewis, J. A. Bruce, D. C. Bookbinder and M. S. Wrighton, *J. Am. Chem. Soc.*, 1982, **104**, 467–482.

7 U. Sim, H.-Y. Jeong, T.-Y. Yang and K. T. Nam, *J. Mater. Chem. A*, 2013, **1**, 5414–5422.

8 K. Novoselov, A. K. Geim, S. Morozov, D. Jiang, M. K. I. Grigorieva, S. Dubonos and A. Firsov, *Nature*, 2005, **438**, 197–200.

9 Y. Liang, Y. Li, H. Wang, J. Zhou, J. Wang, T. Regier and H. Dai, *Nat. Mater.*, 2011, **10**, 780–786.

10 J.-D. Qiu, G.-C. Wang, R.-P. Liang, X.-H. Xia and H.-W. Yu, *J. Phys. Chem. C*, 2011, **115**, 15639–15645.

11 Q. Xiang, J. Yu and M. Jaroniec, *Chem. Soc. Rev.*, 2012, **41**, 782–796.

12 M. G. Walter, E. L. Warren, J. R. McKone, S. W. Boettcher, Q. Mi, E. A. Santori and N. S. Lewis, *Chem. Rev.*, 2010, **110**, 6446–6473.

13 F.-M. Liu, B. Ren, J.-W. Yan, B.-W. Mao and Z.-Q. Tian, *J. Electrochem. Soc.*, 2002, **149**, G95–G99.

14 A. J. Bard and L. R. Faulkner, *Electrochemical methods: fundamentals and applications*, Wiley, New York, 1980.

15 J. D. Benck, Z. Chen, L. Y. Kuritzky, A. J. Forman and T. F. Jaramillo, *ACS Catal.*, 2013, **2**, 1916–1923.

16 Y. Li, H. Wang, L. Xie, Y. Liang, G. Hong and H. Dai, *J. Am. Chem. Soc.*, 2011, **133**, 7296–7299.

17 B. Conway and B. Tilak, *Electrochim. Acta*, 2002, **47**, 3571–3594.

18 T. F. Jaramillo, K. P. Jørgensen, J. Bonde, J. H. Nielsen, S. Horch and I. Chorkendorff, *Science*, 2007, **317**, 100–102.

19 Y. Li, W. Zhou, H. Wang, L. Xie, Y. Liang, F. Wei, J.-C. Idrobo, S. J. Pennycook and H. Dai, *Nat. Nanotechnol.*, 2012, **7**, 394–400.

20 J. R. McKone, E. L. Warren, M. J. Bierman, S. W. Boettcher, B. S. Brunschwig, N. S. Lewis and H. B. Gray, *Energy Environ. Sci.*, 2011, **4**, 3573–3583.

21 P. D. Tran, S. S. Pramana, V. S. Kale, M. Nguyen, S. Yang Chiam, S. K. Batabyal, L. H. Wong, J. Barber and J. Loo, *Chem.–Eur. J.*, 2012, **18**, 13994–13999.

22 L. G. Cancado, A. Jorio, E. H. Martins, F. Stavale, C. A. Achete, R. B. Capaz, M. V. O. Moutinho, A. Lombardo, T. S. kulmala and A. C. Ferrari, *Nano Lett.*, 2011, **11**, 3190.

23 A. Ferrari and J. Robertson, *Phys. Rev. B: Condens. Matter Mater. Phys.*, 2001, **64**, 075414.

24 C. Casiraghi, S. Pisana, K. S. Novoselov, A. K. Geim and A. C. Ferrari, *Appl. Phys. Lett.*, 2007, **91**, 233108.

25 X. Li, W. Cai, J. An, S. Kim, J. Nah, D. Yang, R. Piner, A. Velamakanni, I. Jung, E. Tutuc, S. K. Banerjee, L. Colombo and R. S. Ruoff, *Science*, 2009, **324**, 1312–1314.

26 C. D. Wagner, W. M. Riggs, L. E. Davis, J. F. Moulder and G. E. Muilenberg, *Handbook of X-ray Photoelectron Spectroscopy*, Perkin-Elmer Corporation, USA, 1979.

3664 | *Energy Environ. Sci.*, 2013, **6**, 3658–3664

This journal is © The Royal Society of Chemistry 2013